Turbulent kinetic energy balance in the wake of a self-propelled body

T. Faure, G. Robert

Abstract An experimental study of the turbulent wake of a self-propelled body in a wind tunnel is reported. A significant difference is formed between the turbulent kinetic energy balance in a wake with drag and in the wake of a self-propelled body: the production term is very small in comparison with the other terms of the turbulent kinetic energy balance, and this result seems to be typical of self-propulsion. The axial evolution of the wake radius and turbulent kinetic energy profiles are described. Sufficiently far downstream from the body, a self-similar profile is found. Particular attention is devoted to the turbulent kinetic energy balance; all the terms in the energy balance are evaluated experimentally.

List of symbols

D	diameter of the body
L	axial length scale
l	radial length scale
R	radius of the body
r	radial coordinate
r^*	radius of the wake
U	mean axial velocity scale
$\hat{U}$	defect velocity
U_e	freestream velocity
u	fluctuating velocity scale
x	axial coordinate
ε	dissipation rate
$\eta = r/r^*$	radial relative direction
θ	azimuthal coordinate
v	kinematic viscosity
ρ	density

1
Introduction

Although wakes that spread behind different kinds of bodies have been studied many times (Carmody 1965, Chevray 1968), the development of a turbulent wake behind a self-propelled body is the subject of few publications. In this configuration,

T. Faure, G. Robert
Laboratoire de Mécanique des Fluides et d'Acoustique,
URA CNRS 263 École Centrale de Lyon, F-69131 Écully Cedex, France

Correspondence to: T. Faure

the drag of the body is cancelled by a thrust, so that the momentum integral, which expresses the difference between thrust and drag, is equal to zero and a self-propelled wake is a momentumless one.

Two-dimensional self-propelled wakes have been studied experimentally by Cimbala and Park (1990) and Park and Cimbala (1991) where a momentumless configuration was obtained using jet injection. These authors found self-similarity of the axial and transverse turbulence intensities. The behaviour of turbulence was quite different from that of plane wakes with drag or jets but rather similar to grid turbulence. The type of injection (central or peripheral jet) was found to be an important parameter for the rate of decay of mean velocity and for spreading, however it had no influence on axial turbulence intensity.

Axisymmetric momentumless wakes were first investigated by Schooley and Stewart (1963) in a stratified medium; they observed slower entrainment in the vertical than in the horizontal direction but did not give data for the velocity field inside the wake. The benchmark experimentation for a self-propelled body is that of Naudascher (1965): a circular disk with a coaxial jet at its centre was placed in a wind tunnel at a Reynolds number based on the diameter of the disk of $Re_D = 5.5 \times 10^4$. He pointed out that, whereas the self-similar profiles for simple jets and wakes require only a single amplitude and width scaling, those for the momentumless wake depend on a number of additional normalising scales. The measurement of some of the terms of the turbulent kinetic energy balance led to the conclusion that the production term was very small in comparison with the convection term.

The problem was examined in a more theoretical way by Finson (1975). He used Naudascher's results to show that the far wake behaviour does not become independent of the initial conditions and that there is no natural length scale with which to characterise this region.

A comparison between a propeller-driven slender body and a peripheral-jet model was carried out by Swanson et al. (1974), Chieng et al. (1974) and Schetz and Jakubowski (1975). The Reynolds number was $Re_D = 6 \times 10^5$ and they observed that the wake development of a blunt body driven by a central jet to yield a zero momentum wake was different from the wake of a body driven by a peripheral jet.

Another noteworthy experiment is the investigation in the momentumless wake of an axisymmetric jet-propelled body, by Higuchi and Kubota (1990). They tested the influence of injection and showed that the relaxation zone depended on the turbulence in the initial wake.

The near region of the wake of a momentumless, propeller-driven body was compared with the wake generated by a body with a rotating hub without blades by Hyun and Patel (1992). The Reynolds number was $Re_D = 1.53 \times 10^5$. They processed the velocity measurements in phase with the propeller rotation and observed structures induced by each blade in a region that extended to two diameters downstream of the body.

We now turn our attention to theoretical approaches to the self-propelled wake flow problem. Tennekes and Lumley (1972) discussed the solution analytically far downstream for a two-dimensional momentumless wake. A similar approach was used by Ferry and Piquet (1987) in the axisymmetric case for a propeller-driven body. The problem is more complex than for the jet-driven body because of a tangential mean velocity component that appears in the turbulent kinetic energy equation.

Turbulent kinetic energy balances are available for jets and simple wakes. Wygnanski and Fiedler (1969) experimentally determined all the terms of the balance for an axisymmetric jet. Dissipation was evaluated using a semi-isotropic formulation and pressure transfer was deduced from the balance. Recently, balances of turbulent kinetic energy and Reynolds stresses were produced in axisymmetric jets (Panchapakesan and Lumley 1993, Hussein et al. 1994). A two-dimensional cylinder wake was studied by Browne et al. (1987); they measured all the terms of the balance (except the pressure transfer term) and paid great attention to the dissipation. The nine major terms that make up the total dissipation were measured in the self-preserving region and compared with an isotropic dissipation formulation: the result indicated that the isotropic relation underpredicted the total dissipation by about 30%. These authors found self-similarity for every transport term in the far wake region.

The objective of the present investigation is to provide experimental data for a momentumless, propeller-driven, axisymmetric wake. An experiment was carried out in a wind tunnel and a complete characterisation from the near to the far region obtained. An analysis of the turbulent kinetic energy balance is carried out and we observe that the production term is an order of magnitude smaller than the other terms. In the self-similar zone, all the terms of the turbulent kinetic energy balance are evaluated.

2
Analysis
We consider the wake that develops far downstream from the body. The classical definition of this zone is based on a small velocity defect criterion. Let $\hat{U}$ be the characteristic defect velocity, that is the maximum difference between the free-stream velocity U_e and the axial mean velocity. The small defect criterion is

$$\frac{\hat{U}}{U_e} \ll 1$$

This definition of the far wake is difficult to quantify experimentally because we do not know, a priori, how small the above velocity ratio should be. A more useful working definition of the far region is where there is self-similarity of velocity profiles.

We now turn our attention to the behaviour of turbulence in this self-similar region. The average turbulent kinetic energy is defined as

$$\overline{q^2} = (\overline{u_x^2} + \overline{u_r^2} + \overline{u_\theta^2})/2$$

which satisfies the following equation in cylindrical coordinates for an axisymmetric mean flow with weak swirl:

$$\overline{U}_x \frac{\partial \overline{q^2}}{\partial x} + \overline{U}_r \frac{\partial \overline{q^2}}{\partial r} = -\overline{u_x^2} \frac{\partial \overline{U}_x}{\partial x} - \overline{u_x u_r} \frac{\partial \overline{U}_r}{\partial x} - \overline{u_x u_\theta} \frac{\partial \overline{U}_\theta}{\partial x}$$

$$-\overline{u_x u_r} \frac{\partial \overline{U}_x}{\partial r} - \overline{u_r^2} \frac{\partial \overline{U}_r}{\partial r} - \overline{u_\theta^2} \frac{\overline{U}_r}{r}$$

$$-\overline{u_r u_\theta} \frac{\partial \overline{U}_\theta}{\partial r} + \overline{u_r u_\theta} \frac{\overline{U}_\theta}{r}$$

$$-\frac{\partial \overline{q^2 u_x}}{\partial x} - \frac{\partial \overline{q^2 u_r}}{\partial r} - \frac{\overline{q^2 u_r}}{r}$$

$$-\frac{1}{\rho} \frac{\partial \overline{p u_x}}{\partial x} - \frac{1}{\rho} \frac{\partial \overline{p u_r}}{\partial r} - \frac{\overline{p u_r}}{\rho r}$$

$$+\nu \left(\frac{\partial^2 \overline{q^2}}{\partial x^2} + \frac{\partial^2 \overline{q^2}}{\partial r^2} + \frac{1}{r} \frac{\partial \overline{q^2}}{\partial r} \right) - \varepsilon \qquad (1)$$

A simplified form can be obtained using the boundary layer approximation, which is based on an analysis of the order of magnitude of each term of the above equation (Corrsin 1963). Characteristic length and velocity scales are chosen and order of magnitude relations between these scales deduced from the continuity and momentum equations. In our problem, all terms in the equations of motion can be estimated using four independent scales:

- L the axial length scale ($\sim x$)
- l the radial length scale ($\sim r^*$, the wake width)
- U the mean axial velocity scale ($\sim U_e$)
- u the fluctuating velocity scale

In the far wake, we have $l/L \ll 1$ and $u/U \ll 1$ with both these ratios going to zero as x tends to infinity. This leads to the following dominant terms in the turbulent kinetic energy equation:

$$\overline{U}_x \frac{\partial \overline{q^2}}{\partial x} = -\overline{u_x u_r} \frac{\partial \overline{U}_x}{\partial r} - \overline{u_r u_\theta} \left(\frac{\partial \overline{U}_\theta}{\partial r} - \frac{\overline{U}_\theta}{r} \right) - \frac{1}{r} \frac{\partial}{\partial r} (r \overline{q^2 u_r}) - \frac{1}{\rho r} \frac{\partial}{\partial r} (r \overline{p u_r}) - \varepsilon$$

$$\left(\frac{U}{u} \frac{l}{L} \right) \frac{u^3}{l} \qquad \left(\frac{u}{U} \frac{L}{l} \right) \frac{u^3}{l} \qquad \left(\frac{u}{U} \frac{L}{l} \right) \frac{u^3}{l} \qquad \frac{u^3}{l} \qquad \frac{u^3}{l} \qquad \frac{u^3}{l}$$

$$\underbrace{\qquad}_{\text{convection}} \quad \underbrace{\qquad\qquad\qquad\qquad}_{\text{production}} \quad \underbrace{\qquad}_{\text{kinetic transfer}} \quad \underbrace{\qquad}_{\text{pressure transfer}} \quad \underbrace{\qquad}_{\text{dissipation}} \qquad (2)$$

The order of magnitude of each term retained in the balance is noted in equation (2). Since, a priori, the relative magnitudes of the small quantities $l/L \ll 1$ and $u/U \ll 1$ are unknown, those terms which contains factors of their ratio,

$$K = \frac{u}{U}\frac{L}{l} \tag{3}$$

have been retained. For a drag wake, it is known that K tends to a constant value in the far wake. For a momentumless wake, we can argue that K ought also to tend towards a constant value as x tends to infinity, by appeal to the principle of the least degeneracy from the theory of asymptoties. Of course, this is not an argument that can be proved because the latter principle is only a rule of thumb. Nonetheless, a constant value of K is formed experimentally in the far wake. If we accept this, then all terms in (2) would appear to be necessary. In fact, we shall see, the numerical value of K turns out to be small and the term on the left of (2) dominates over the first two terms on the right.

For a drag wake, we can use conservation of momentum in the far wake to show that

$$\int_0^\infty rU_e(U_e - \overline{U}_x)\,\mathrm{d}r = \mathrm{const} \tag{4}$$

and this relation allows derivation of the overall properties of self-similarity. However, for the momentumless wake the constant is zero and Eq. (4) yields no useful result. To resolve this difficulty, a less obvious relation was established by Tennekes and Lumley (1974) in the plane case and by Ferry and Piquet (1987) for an axisymmetric flow. These authors use the equation for the axial mean velocity to show that

$$\int_0^\infty r^3 U_e(U_e - \overline{U}_x)\,\mathrm{d}r = \mathrm{const} \tag{5}$$

for a momentumless far wake. The order of magnitude relation for mean velocity defect is

$$\hat{U} = \frac{u^2}{U}\frac{L}{l} \tag{6}$$

which follows from the order of magnitude analysis of the equations of motion mentioned before Eq. (2). Then, Eq. (5) leads to the relation:

$$l^3 u^2 L = \mathrm{const} \tag{7}$$

which, with (3) gives

$$u = \mathrm{const} \times \left(\frac{U^3 K^3}{L^4}\right)^{1/5} \tag{8}$$

and

$$l = \mathrm{const} \times \left(\frac{L}{U^2 K^2}\right)^{1/5} \tag{9}$$

If we now use constancy of K, $U = U_e$, $L = x$, and $l = r^*$, we have

$$u \sim x^{-4/5}, \qquad r^* \sim x^{1/5} \qquad \hat{U} \sim x^{-4/5} \tag{10}$$

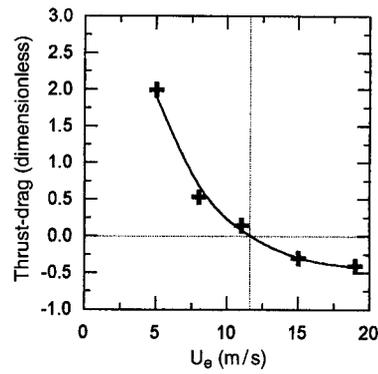These results are well known in the existing literature (Tennekes and Lumley 1974).

Fig. 1. Variation of the thrust-drag balance (dimensionless) with the freestream velocity

3
Experimental arrangements

The wake is generated by an axisymmetric, streamlined body, mounted in the working section of a wind tunnel (500 mm × 500 mm, 6 m long). The experimental freestream velocity can vary from 5 to 80 m/s with a uniformity of $\pm 2\%$ and a maximum turbulence intensity of 0.7%. The model has a diameter $D = 8$ cm and a length of 50 cm. It has an elliptical nose, a cylindrical middle section and a conical stern. The propulsion system consists of a three-blade marine type propeller with a diameter of 4 cm. The inside of the body is hollow and contains the motor (Minimotor SA BLD 568 type, 15 000 rpm maximum speed) which drives the propeller. An electronic system is available to control the rotation speed. A support having a symmetrical NACA $66_1 012$ profile with a chord of 10 cm and a maximum width of 1.2 cm was chosen to minimise aerodynamic perturbations around the body. Electrical wires for power supply and speed regulation are mounted inside this support. An alignment system allows the model to be oriented with the freestream flow. Once this adjustment is made, the angle between the wake axis and the tunnel axis was found to be less than 0.3°.

For a self-propelled body, the drag generated by the model equals the thrust created by the propulsion system. To bring about this state a momentum balance was established for the model. To this effect, we have two parameters which can vary, the freestream velocity and the propeller rotation speed. The momentum balance need the measurement of velocity and pressure, and these quantities were determined with a five-hole pressure probe. Note in Fig. 1 that the thrust-drag balance is normalized by the upstream momentum flux. The propeller rotation was fixed at its maximum value and the freestream velocity was varied to make the drag equal to the thrust. Self-propulsion was realised with a freestream velocity of 11 m/s.

The measurements are made in a closed wind tunnel and wakes are easily influenced by pressure gradients. Nevertheless, this pressure effect is small, as it is shown in Fig. 2; the momentum flux, plotted with the same scale as in Fig. 1 for comparison, is constant with axial distance.

The flow is three-dimensional and turbulent; it is therefore necessary to use a directional probe that can measure both the mean and the fluctuating parts of the velocity. An automated
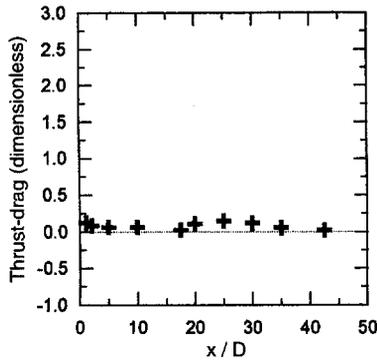
Fig. 2. Variation of the momentum flux (dimensionless) with the axial distance

triple hot-film anemometry system was developed that gives all three components of instantaneous total velocity. The probe is a Dantec 55R91 type, with an active length of 0.8 mm. It has a nickel film deposited on a quartz cylinder, 70 μm in diameter. The three film supports are orthogonal and inserted into a sphere of 2 mm diameter. Calibration of each sensor was performed in the unperturbed freestream. Periodic verification was carried out during the acquisition procedure: the probe was placed in the freestream from time to time and a calibration point obtained for each film. As part of the signal processing, such points were used to update the calibration curve. This procedure is used to avoid any change in the ambient temperature.

The films were operated as constant temperature anemometers at an overheat ratio of 0.7. Output voltages from the anemometers were passed through offset and gain circuits, before low-pass filtering with a cut-off frequency of 2 kHz. They were then digitised at a sampling frequency of 4 kHz per channel using a 12 bit A-D converter. The data were stored on the hard disk of a 80 386 PC computer for later processing. Sample of at least 20 s was necessary to obtain convergence of the averages for third order moments of fluctuating velocity.

A complete investigation in a plane perpendicular to the wake axis was performed for several axial distances from the near to the far wake. The Reynolds number based on the diameter of the body and the freestream velocity was $Re_D = 5.8 \times 10^4$.

4
Experimental determination of the turbulent kinetic energy balance

The method used to experimentally determine the turbulent kinetic energy balance is similar to the one described by Browne et al. (1987). Measurements were made of all the terms of Eq. (2) except for the pressure transfer term which was determined from the overall balance. The axial turbulent kinetic energy gradient, appearing on the left of Eq. (2), is defined from the self-similar form:

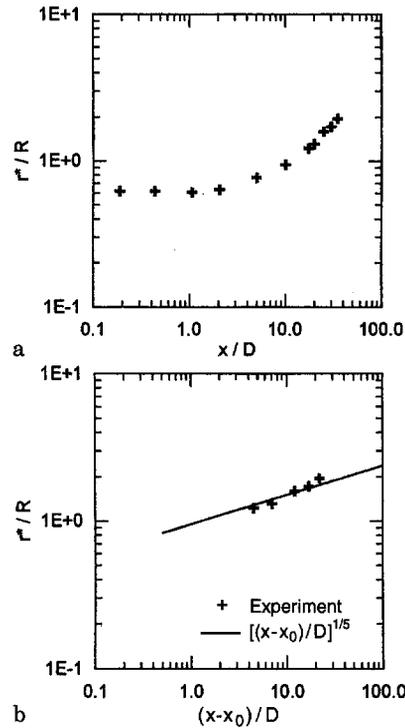$$\overline{q^2} = \overline{q_m^2}(x/D)\,h(\eta) \tag{11}$$

Fig. 3. a Axial variation of the radius of the wake from the trailing edge of the body; b axial variation of the radius of the the wake from its virtual origin

where $\overline{q_m^2}$ is the maximum value of $\overline{q^2}$ at station x and $\eta = r/r^*(x/D)$ the radial similarity variable. Thus,

$$\frac{\partial \overline{q^2}}{\partial x} = \left[\frac{d\overline{q_m^2}}{dx}(x/D)\,h(\eta) - \overline{q_m^2}(x/D)\frac{\eta}{r^*}\frac{dr^*}{dx}(x/D)\frac{dh}{d\eta}(\eta)\right]/D \tag{12}$$

A least-square spline fit was first applied to the data on $h(\eta)$ before numerical differentiation yielding to $d\,h/d\,\eta$. The radial derivatives of $\overline{U_x}$, $\overline{U_\theta}$ and $r\,\overline{q^2u_r}$ were obtained in a similar way. The three third order moments of the $\overline{q^2u_r}$ term could be measured directly, thanks to the triple hot film probe. The dissipation term was evaluated using the classical isotropic formulation:

$$\varepsilon = 15\,\nu\left(\overline{\frac{\partial u_x}{\partial x}}\right)^2 \tag{13}$$

in which the axial gradient term was evaluated using Taylor's hypothesis and the time derivative of the velocity fluctuation:

$$\varepsilon = \frac{15}{\overline{U_x^2}}\,\nu\left(\overline{\frac{\partial u_x}{\partial t}}\right)^2 \tag{14}$$

5
Results

The measurements were carried out over a wide range of axial positions ($0.19 \leqslant x/D \leqslant 50$, $x = 0$ being at the trailing edge of the body). The radius of the wake r^* was defined as the location at which the axial turbulence intensity had fallen to half of its maximum value. Its axial evolution is plotted in Fig. 3a and
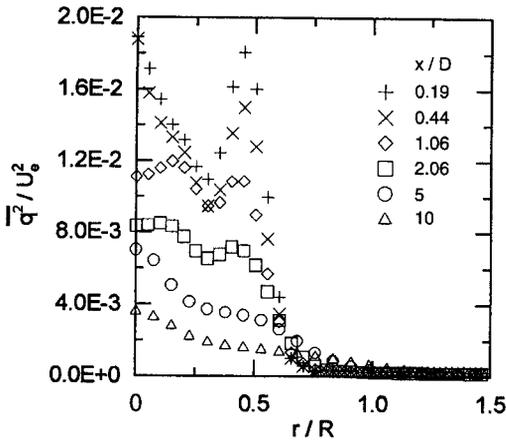
Fig. 4. Radial variation of the turbulent kinetic energy for $x/D \leqslant 10$
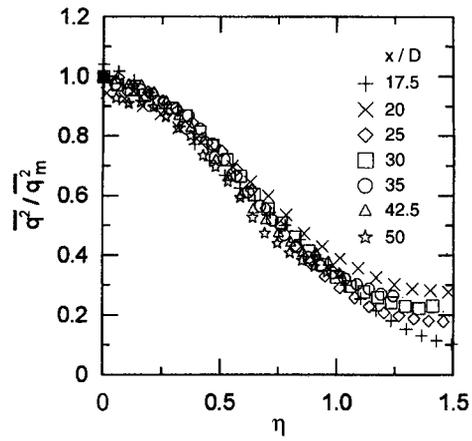

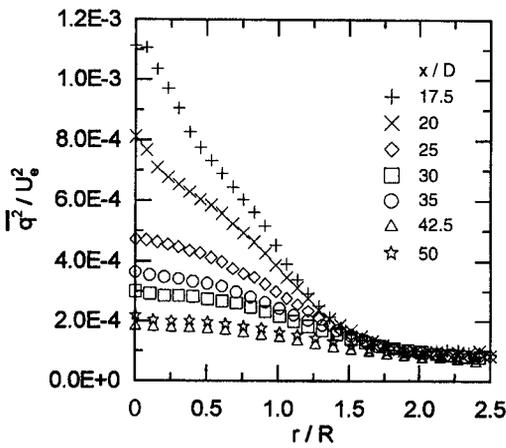Fig. 6. Self-similar profile for the turbulent kinetic energy

Fig. 5. Radial variation of the turbulent kinetic energy for $x/D \geqslant 17.5$
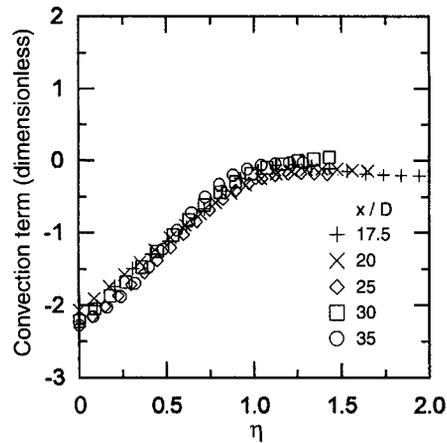

Fig. 7. Self-similar form of the convection term (dimensionless)

shows three different regions: the near wake where r^* is nearly constant, the establishment zone between $2 < x/D < 10$, and the far wake in which the behaviour has the asymptotic power law form. The virtual origin of the wake was determined by fitting the maximum turbulent kinetic energy to a self-similar power law in $x - x_0$. A least-squares method was used, leading to the virtual origin $x_0/D = 13$. With this correction, the asymptotic law for an axisymmetric, self-propelled body, with r^* proportional to $(x - x_0)^{1/5}$ is found (Fig. 3b).

Turbulent kinetic energy profiles are plotted for different axial positions in Figs. 4 and 5. We observe that the overall level decreases with axial distance in the wake. For this reason, it has been necessary to represent the evolution using two plots with a different scale. The turbulent kinetic energy shows two peaks in the near wake region, associated with the hub ($r/R \sim 0$ to 0.15) and the tip ($r/R = 0.5$) of the propeller blades. The higher level of turbulence is due to the emission of a horseshoe vortex on the hub and a tip vortex for each blade. The secondary peak vanishes for $x/D > 5$ and the primary one becomes a central maximum.

In Fig. 6, the turbulent kinetic energy has been scaled by its local maximum value and the radial coordinate scaled on the radius of the wake. It will be noticed that the form is the same

for any axial position, illustrating self-similarity of turbulent kinetic energy.

We can obtain a more precise definition of the constant K if we take $U = U_e$, $L = x$, and $l = r^*$ as the scales in Eq. (3). It is then found experimentally that $K \approx 0.05$, which is small and leads to negligible values for the first two terms on the right hand side of Eq. (2), which both contain factors of K in their order of magnitude estimates. Thus, to a good approximation, the energy balance in the momentumless far wake is described by:

$$\overline{U}_x \frac{\partial \overline{q^2} x}{\partial x} = -\frac{1}{r} \frac{\partial}{\partial r} (r \overline{q^2 u_r}) - \frac{1}{\rho r} \frac{\partial}{\partial r} (r \overline{p u_r}) - \varepsilon \qquad (15)$$

This equation expresses the fact that, in contrast with the case of a drag wake, the production terms are small and can be neglected.

The convection term, normalised by $\overline{q^2}^{3/2}/r^*$, is plotted in Fig. 7 for the far wake. Self-similarity is evident since the same curve is found for any axial distance $x/D \geqslant 17.5$. The same result is found for the other terms of the turbulent kinetic energy equation.

All the terms in (2) are given for the self-similar momentumless wake with weak swirl in Fig. 8. Note that in this
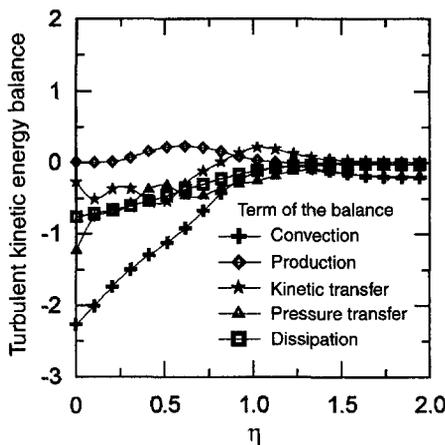
Fig. 8. Self-similar form of the turbulent kinetic energy balance (dimensionless) in the momentumless far wake
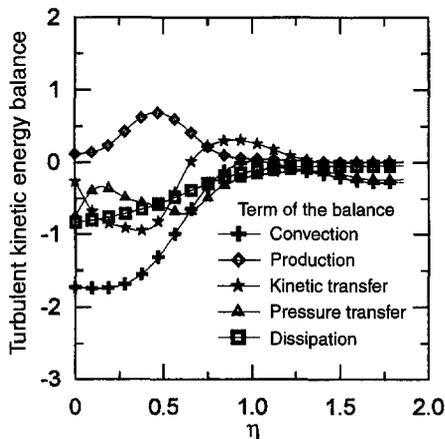

Fig. 9. Self-similar form of the turbulent kinetic energy balance (dimensionless) in the far wake of the same body without propeller

equation, the balance is written as an equilibrium between convection on the left hand side, and other transfers on the right hand side. As a result, a convection input of energy appears as a negative contribution in the balance, unlike the other terms. If one looks more closely at the radial variation of the overall turbulent kinetic energy balance, on the centreline of the wake, energy input is due to convection, while losses result from dissipation and kinetic and pressure transfers. As distance from the centreline increases, the magnitude of convection tends to decrease but remains the largest term in the balance. The kinetic transfer becomes positive in the outer part of the wake, where it represents an input of kinetic energy due to radial transport. The measurement of the production term validates the previous analysis that brings to (15).

Although a wake is a decaying turbulent flow, and as a consequence, all the transfers are decreasing in magnitude with axial distance, the relative part of these transfers in the turbulent kinetic energy balance remains the same. This is provided with the dimensionless self-similar form. The observation that the production term is negligible in comparison with other

transfers could not be related to a decaying turbulence but to the momentumless relation (5). This result, previously observed for axisymmetric or two-dimensional jet-driven wakes, seems to be typical of the self-propelled bodies. In fact, for a drag-body wake, production is not small as shown in Fig. 9 (Faure 1995), but is the same order in magnitude as dissipation (see also Browne et al. 1987 for the two-dimensional case).

6
Conclusion

The turbulent far wake of a self-propelled body behaves in a different way than a drag wake. A velocity excess is characteristic of this kind of flow and the propeller-driven configuration considered here has a swirl component (in θ) that is not present for a jet-driven body. Self-similarity of the turbulent kinetic energy profile is found for any axial distance $x/D \geqslant 17.5$. All the terms of the turbulent kinetic energy equation are measured in this flow, which is an original set of data provided from this study. A main result of this investigation is that self-similarity of the turbulent kinetic energy balance is found experimentally in the far wake, by measurement of all the terms appearing in the balance. An important conclusion is that production of turbulent energy is negligible in comparison to the other transfer terms, a result which is typical of self-propulsion. This fact was previously established for a jet-driven two dimensional body wake (Cimbala and Park 1990) and for a jet-driven axisymmetric body wake (Naudascher 1965). In a drag wake, production and dissipation are of the same order of magnitude. In a momentumless wake the simple balance between production and dissipation no longer exists and this is a reason why turbulence models fail to predict this flow correctly. This result has been suggested by order of magnitude analysis of the energy equation based on the boundary layer approximation in the case of self-propulsion with limited experimental input, and confirmed by the detailed measurements.

273

References

Browne LWB; Antonia RA; Shah DA (1987) Turbulent energy dissipation in a wake. J Fluid Mech 179: 307–326

Corrsin S (1963) Turbulence: experimental methods. In: Handbuch der Physik. Vol. 8, Part 2 pp 524–590, Berlin: Springer-Verlag

Carmody T (1964) Establishment of the wake behind a disk. Trans ASME D J Basic Engng 87: 869–882

Cimbala JM; Park WJ (1990) An experimental investigation of the turbulent structure in a two-dimensional momentumless wake. J Fluid Mech 213: 479–509

Chevray R (1968) The turbulent wake of a body of revolution. Trans ASME D J Basic Engng 90: 275–284

Chieng CC; Jakubowski AK; Schetz JA (1974) Investigation of the turbulent properties of the wake behind self-propelled, axisymmetric bodies: Office of Naval Research, VPI-Aero-025, Sept. 1974, available through NTIS

Faure T (1995) Étude expérimentale du sillage turbulent d'un corps à symétrie de révolution autopropulsé par hélice. PhD Thesis, No 95-01, École Centrale de Lyon

Ferry M; Piquet J (1987) Sillage visqueux lointain d'un corps sous-marin autopropulsé. Report DRET 86 1201, SIREHNA

Finson ML (1975) Similarity behaviour of momentumless turbulent wakes. J Fluid Mech 71 (3): 465–479

Higuchi H; Kubota T (1990) Axisymmetric wakes behind a slender body including zero-momentum configurations. Phys Fluids A 2 (9): 1615–1623

Hussein HJ; Capp SP; George WK (1994) Velocity measurements in a high-Reynolds-number, momentum-conserving, axisymmetric, turbulent jet. J Fluid Mech 258: 31–75

Hyun BS; Patel VC (1991) Measurements in the flow around a marine propeller at the stern of an axisymmetric body. Part 1: Cicumferentially-averaged flow, Part 2: Phase-averaged flow. Exp Fluids 11: 33–44 105–117

Naudascher E (1965) Flow in the wake of self-propelled bodies and related sources of turbulence. J Fluid Mech 22 (4): 625–656

Panchapakesan NR; Lumley JL (1993) Turbulence measurements in axisymmetric jets of air and helium. Part 1. Air jet, Part 2. Helium jet. J Fluid Mech 246: 197–247

Park WJ; Cimbala JM (1991) The effect of jet injection geometry on two-dimensional momentumless wakes. J Fluid Mech 224: 29–47

Schetz JA; Jakubowski AK (1975) Experimental studies of the turbulent wake behind self-propelled slender bodies. AIAA J 13 (12): 1568–1575

Schooley AH; Stewart RW (1963) Experiments with a self-propelled body submerged in a fluid with a vertical density gradient. J Fluid Mech 15 (1): 83–99

Swanson Jr RC; Schetz JA; Jakubowski AK (1974) Turbulent wake behind slender bodies including self-propelled configurations. Office of Naval Research, VPI-Aero-024, Sept. 1974, available through NTIS

Tennekes H; Lumley JL (1974) A first course is turbulence. Cambridge, MA: MIT Press

Wygnanski I; Fiedler H (1969) Some measurements in the self-preserving jet. J Fluid Mech 38: 577–612